Article:

Becque, J. and Wilkinson, T. (2017) The capacity of grade C450 cold-formed rectangular hollow section T and X connections: An experimental investigation. Journal of Constructional Steel Research, 133. pp. 345-359. ISSN 0143-974X

https://doi.org/10.1016/j.jcsr.2017.02.032

THE CAPACITY OF GRADE C450 COLD-FORMED RECTANGULAR HOLLOW SECTION T AND X CONNECTIONS: AN EXPERIMENTAL INVESTIGATION

By

Jurgen Becque[1]

The University of Sheffield, Sheffield, South Yorkshire, UK

Tim Wilkinson

The University of Sydney, Sydney, New South Wales, Australia

[1] corresponding author; address: Sir Frederick Mappin Building, Mappin Street, Sheffield S1 3JD, UK; email: j.becque@sheffield.ac.uk; t: +44 (0)114-2220252.

Abstract:

The paper presents the results of an experimental program which consists of 15 T and X truss joints fabricated from grade C450 cold-formed Rectangular Hollow Sections (RHS). The aim is to study the effect of the increased yield stress and the somewhat reduced ductility resulting from the cold-working process on the static capacity of these joints. The experimental program was designed to include the full range of possible failure modes and covers a comprehensive spectrum of geometries, including commercially available sections which fall outside the CIDECT limits in terms of wall slenderness ratios. In a next step, the results are compared to the current CIDECT design rules where applicable. In particular, the need for a reduction factor of 0.9 on the capacity of grade C450 connections, imposed by both the CIDECT rules and the Eurocode, is evaluated.

1. **Introduction**

The aim of the presented research was to investigate the static capacity of Rectangular Hollow Section (RHS) T and X truss joints made of grade C450 steel. These sections are cold-rolled and possess a nominal yield stress of 450 MPa. Two separate issues thereby required consideration and provided the justification for the new research.

First, it is well-known that the cold-rolling process significantly affects the material properties. While a generally enhanced yield stress is obtained (with the maximum enhancement encountered in the zones of highest cold-working, i.e. the corners), a reduction in ductility (reflected in the strain at rupture) is typically observed. Simultaneously, a reduction in the ratio f_u/f_y, where f_u is the tensile strength and f_y is the yield stress, is to be expected after cold-working the material. It is thereby noted that a slightly more rounded stress-strain curve with a more gradual transition into yielding typically results from cold-working (as opposed to the bilinear curve usually encountered in hot-rolled products) and that, therefore, f_y, within the context of this paper, is to be interpreted as the 0.2% proof stress. The f_u/f_y ratio is of primary importance for failure modes which are governed by fracture. For T and X joints these encompass: 1. punching shear failures, and 2. effective width failures in tension. While the tensile strength f_u obviously plays a primordial role in these phenomena, the corresponding CIDECT design rules (Packer et al. 2009), somewhat illogically, are based on the yield stress of the material f_y, thus necessitating an additional restriction on the f_u/f_y ratio in order to maintain sufficient safety at the ultimate limit state. For grades 355 MPa and below, the CIDECT guidelines have traditionally stated throughout their consecutive versions that the f_u/f_y ratio should exceed 1.2. The most recent version of the rules, comprised in the CIDECT Design Guide 3 (Packer et al. 2009) and also mirrored in the recommendations of the International Institute of Welding (IIW 2009) has extended the range of applicability of the design rules to yield strengths of up to 460 MPa. However, in a similar philosophy, they stipulate that the minimum of f_y and $0.8f_u$ has to be substituted for f_y in the design rules when applying them to higher grade connections. In this respect it should also be noted that the AISC Design Guide 24 for Hollow Structural Section Connections (Packer et al. 2010) conservatively does not yet allow for the use of steel grades with a yield stress beyond 355 MPa.

It is equally important to consider the effect of the higher yield stress on the connection deformations. The CIDECT design rules are implicitly based on a chord wall deformation limit of 3% of b_0, where b_0 is the chord width (Lu et. al 1994). This limit is essentially a serviceability limit. However, it is longstanding CIDECT practice to incorporate this limit directly into the connection capacity equation, rather than providing a separate serviceability check. One could put forward the argument that a C450 connection typically will be subject to higher stresses (and thus higher elastic deformations) near failure than a grade 355 connection and that, thus, the deformation limit is more likely to become the governing factor limiting the connection capacity. Consequently, one might not get the full benefit from increasing the material yield stress to 450 MPa. However, the problem is more complex than this somewhat simplistic view would suggest since, for instance in the case of chord face plastification, large deformations exceeding the 3% limit may not occur until partial plastification of the chord face has taken place and a pattern of yield lines is in the process of developing. Large deformations and the onset of plasticity are often linked and, consequently, violation of the 3% rule may be deferred to higher loads in higher grades of steel. Additionally, the occurrence of a more rounded stress-strain curve, increased residual stresses and uneven work-hardening across the section in cold-rolled RHS all add to the complexity of the problem. CIDECT Design Guide 3 (Packer et al. 2009) specifies a reduction factor of 0.9 to be applied to the capacity of connections in grades beyond 355 MPa (and up to 460 MPa) in order to account for the 'larger deformations' in these connections. The Eurocode (EN 1993-1-8 2005) prescribes the same reduction factor for this range of material strengths. It is obvious, however, that this reduction factor of 0.9 at least partially eliminates the benefits of using higher grade steel, and some controversy surrounds its necessity.

It is also an issue of debate whether it is necessary to apply both a. the upper limit of $0.8f_u$ on f_y, and b. the reduction factor of 0.9 simultaneously and indiscriminately to all connections (as the current CIDECT rules require). Rather, suggestions circulate within the research community to apply specification (a.) only to those failure modes governed by brittle fracture (punching shear and effective width failures in tension) and specification (b.) only to those failure modes which typically exhibit large deformations (chord face plastification and side wall failures). Alternatively, only the reduction factor of 0.9 (and not the upper limit on f_y) could be specified to account for both increased deformations and reduced f_u/f_y ratios. This seems to be the logic adhered to by the Eurocode (EN 1993-1-8 2005), which does not specify a lower limit on f_u/f_y (Wardenier and Puthli, 2011).

Apart from the specific material issues related to the cold-forming process, the research project on C450 connections described in this paper needed to consider the effects of cross-section geometry, in particular the wall slenderness values. The CIDECT design rules, throughout their evolution, have always placed restrictions on the slenderness values of b/t and h/t of the connecting members, where t is the wall thickness, b is the cross-section width (measured perpendicular to the plane of the connection) and h is the cross-section height. Until recently, an upper limit of 35 was maintained on the wall slenderness of both brace and chord members. However, based on re-evaluation of numerical work by Yu (1997) on T and X joints and by Koning & Wardenier (1976) on K gap joints, the most recent version of CIDECT Design Guide 3 (Packer et al. 2009) has extended the wall slenderness limit to 40. In addition, however, compressive brace or chord members need to satisfy at least Class 2 requirements. According to EN 1993-1-1 (and assuming an inside corner radius of 1.5t) this reduces the allowable b/t or h/t ratios to about 32 for grade 450 steel. It is also noted that various design standards around the world, e.g. EC3 EN1993-1-8 (2005) and the AISC Design Guide 24 (Packer et al. 2010), are still maintaining the slenderness limit of 35 in combination with a minimum Class 2 requirement for compressive brace members.

Due to advances in manufacturing techniques it is now possible to produce RHS with wall thicknesses of up to 16 mm by cold-rolling. Consequently, it would be incorrect to exclusively think of cold-rolled RHS as sections with high width-to-thickness ratios. Nevertheless, when inspecting the catalogue of C450 RHS which are commercially on offer in Australia, it is clear that a significant number of products do not satisfy the current CIDECT slenderness limit of 40. Examples of commercial SHS and RHS exceeding this limit are shown in Table 1 and Table 2, respectively. SHS with b/t ratios up to 50 are encountered (SHS 100x100x2), while various RHS possess slenderness values exceeding 60 (RHS 150x50x2.5, RHS 125x75x2, RHS 100x50x1.6) and in a single case reaching 75 (SHS 150x50x2). Although these slender cross-sections were not the exclusive focus of this investigation, some cross-sections with a wall slenderness outside of the CIDECT rules were included in the test program, in order to increase our understanding of their behaviour and aim to extend the current slenderness limits even further over time.

2. **Previous research**

A rather limited volume of previous research is available on Circular Hollow Section (CHS) connections or RHS connections with yield strengths exceeding 355 MPa.

Kurobane (1981) conducted research on CHS K gap connections made of S460 and found that the ultimate capacity in relative terms (i.e. after accounting for the increased yield stress) was 18% lower compared to the same connections in S235. This research at the time did not yet incorporate the 3% deformation limit, but it provided a first indication that a reduction factor on the connection capacity might be in order. Kurobane's findings were later confirmed by Noordhoek et al. (1996) who demonstrated that CHS K gap connections in S460 had lower connection efficiencies than the corresponding S235 connections, even when an effective yield stress of $0.8f_u$ was used. Puthli et al. (2010), however, carried out tests on CHS S460 X connections and observed that for nearly all the connections tested, the experimentally determined capacity exceeded the CIDECT predicted capacity calculated without the 0.9 reduction factor. Numerical analyses followed the tests and suggested that, while there is some justification for the inclusion of a reduction factor, the current value of 0.9 is conservative for S460 X connections. Since punching shear failures were included, the parametric studies also (unsurprisingly) revealed a dependence of the capacities on the f_u/f_y ratio.

On the topic of RHS connections, Mang (1978) conducted early research on high strength S690 K connections and observed a relative reduction in strength of about 1/3 compared to S235 connections. To increase the available data, Liu and Wardenier (2004) carried out further numerical studies on S460 K gap connections and, taking into account the 3% b_0 deformation limit, concluded that a reduction factor of 0.9 on the capacity should be used.

In summary, it appears that the evidence in favour of a 0.9 reduction factor on the capacity of S460 connections almost exclusively results from studies on CHS or RHS K gap connections. On the other hand, only weak or even disproving evidence can be found for the inclusion of this factor for X or T connections. A (re)assessment of the necessity of the reduction factor for T and X connections is part of the aims of this experimental investigation.

Very limited previous research is available on connections with chord or brace members outside the CIDECT wall slenderness limits. However, Fleischer and Puthli (2008) conducted some very noteworthy experimental research in this area. A total of 39 tests were carried out on symmetric K gap connections. Chord members were selected with slenderness values $2\gamma = h_0/t_0$ which exceeded

35 in all cases but two, and ranged up to 52 (it is thereby noted that h_0 is the chord depth and t_0 is the chord wall thickness). In addition, the minimum gap sizes prescribed by CIDECT were not adhered to and were taken as small as $4t_0$, this distance deemed by the authors to be the minimum practical distance for welding. It was concluded, first of all, that the reduced gap size required a re-evaluation of the effective length for punching shear, as a result of the generally increased stiffness of the gap region. It was also observed that, because of the increased slenderness of the chord walls, chord side wall buckling often overtook chord face plastification as the governing failure mode. Since chord side wall buckling is currently not a recognized failure mode for K gap connections in the CIDECT equations, Fleischer and Puthli recommended using the side wall failure equation for Y connections instead. A statistical reliability analysis according to EN 1990 (2002) was also carried out and it was found that a reduction factor of 0.71 on the current CIDECT predicted capacities should be used for the case of chord face plastification and a reduction factor of 0.79 for the case of effective width failures in the brace. These reduction factors simultaneously account for the gap size *and* the chord wall slenderness being outside the CIDECT specifications. The 3% b_0 deformation limit was accounted for in the analysis. It should also be noted that all test specimens were manufactured of S355 steel, except for four of them which were of grade S460. These four tests were not considered separately, rather the statistical analysis was carried out on the complete pool of S355 and S460 data.

3. **Material properties**

The experimental program described in this paper included a total of 15 C450 connections. As part of the investigation, 24 coupons were taken from left-over segments of the same RHS tubes used to manufacture the test specimens. The coupons were tested according to the AS/NZS1391 (1991) specifications. For each RHS one coupon was taken from the middle of the face opposite the longitudinal seam weld and one coupon was taken from the middle of a face adjacent to the weld face, as illustrated in Figure 1. All coupons were 20 mm in width and were tested at a strain rate of $5x10^{-4}$/s in a 300 kN capacity MTS Sintech universal testing machine.

All RHS used in the test program are commercially available in Australia. However, their origins could be traced to two different sources: all sizes up to 200x200x6 were rolled in Australia by OneSteel Australian Tube Mills, while the larger sizes were imported from Japan. Slightly different material properties can therefore be expected in these two groups of RHS, although all sizes are sold as grade C450 in Australia, conforming to AS/NZS 1163 (2009).

Table 3 lists the yield stress f_y (taken as the 0.2% proof stress) and the tensile strength f_u obtained from all coupon tests. The reported values were obtained after eliminating strain rate dependent effects by repeatedly halting the test and allowing the load to settle for about 2 minutes. A reduction factor equal to the ratio of the load right before halting the test to the load right before resuming the test was then applied to the stress measurements.

As a representative example, Figure 2 shows the full stress-strain curves of the coupons taken from the SHS200x200x6 tube. Engineering stresses and strains are presented. The material in the face opposite the weld generally exhibited a slightly higher yield stress than the material in the face adjacent to the weld, while the tensile strengths in both faces were similar. This can be explained by the larger amount of work-hardening undergone by the face opposite the weld during the fabrication process.

As pointed out in the introductory literature review, the f_u/f_y ratio of the material is of particular interest. For the Australian made sections, an average yield stress f_y of 435 MPa was measured, in combination with a tensile strength f_u of 511 MPa, resulting in: f_u/f_y = 1.18. For the Japanese made sections, on average f_y reached 459 MPa and f_u equalled 537 MPa, and thus: $f_u/f_y = 1.17$. Therefore, the materials narrowly failed the CIDECT requirement that f_u/f_y has to exceed 1.2.

4. **Welding**

All welding was carried out according to AS/NZS 1554.1 (2000) by a welder certified to these standards. In particular, the welding speed and heat input adhered to the limits set by AS/NZS 1554.1. Complete welding records of all test specimens are available in Becque et al. (2011). Gas metal arc welding with W503 electrode wire (brand name: CIGWELD Autocraft LW1-6) was selected for all welds. Argon UN1006 was used as a shielding gas and before welding the inside of the brace members was purged using Argon UN1956.

Since the aim of the project was to investigate the applicability of the CIDECT design rules to C450 steel connections, failure preferably needed to take place within the tube steel and any type of weld failure was considered undesirable. Therefore, full penetration butt welds with superimposed fillet welds (Fig. 3a) were selected wherever possible and designed not to be the critical components. The pre-qualified weld details presented in AS/NZS 1554.1 (2000) were used whenever possible. The decision to select a compound weld was reinforced by findings that it is difficult to obtain full penetration at the root of the weld in thicker tubes (Wardenier et al. 2009, Becque and Cheng 2016), a conclusion which was also drawn from welding two practice connections, slicing through the welds and visually inspecting the etched welds. Figure 3 shows some of the weld details which were used in various connections. The use of a backing plate was necessary for the larger size equal-width connections (X10 and X11, with chord sizes of SHS 250x250x10 and SHS 300x300x8, respectively) (Fig. 3g).

5. **Test program and set-up**

The experimental program encompassed a total of 15 connection tests, including 4 T joints and 11 X joints. The experiments can be divided into two separate categories:

1. Connections which fell within the current geometric limits set by the CIDECT rules (Packer et al. 2009). These limits mostly relate to the brace and chord slenderness values h_0/t_0, b_0/t_0 (=2γ), h_1/t_1 and b_1/t_1 (where h_0, b_0, t_0, h_1, b_1 and t_1 are illustrated in Figure 4), but also apply to the aspect ratio h_1/b_1, the ratio β (= b_1/b_0) and the brace angle θ. These tests highlighted the effects of the increased yield strength and the somewhat reduced f_u/f_y ratio of the C450 steel on the connection behaviour and capacity and aimed to answer the question whether the current CIDECT rules (possibly with modification factors) can be applied to C450 connections.
2. Connections of which the brace and/or chord wall slenderness values exceeded the current CIDECT limitations. Given that a significant portion of the SHS/RHS in the available C450 product range falls outside these limitations, the authors felt that it was important to include some of these sizes in the experimental program. The availability of experimental data will thereby provide a foundation to further extend the range of applicability of the design equations towards more slender hollow sections in the future.

An overview of the complete experimental program is provided in Table 4, where the connections involving more slender sections (category 2) are highlighted. A wide range of geometries were included in the test program, with brace sizes ranging from SHS 75x75x5 to SHS 300x300x8 and chord sizes ranging from SHS 125x125x5 to SHS 400x400x16. Square as well as rectangular hollow sections were included and, as summarized in Table 4, a wide range of geometric parameters β (= b_1/b_0), 2γ (= b_0/t_0), τ (=t_1/t_0) and θ were considered. In particular, the maximum value of the chord face slenderness 2γ was 50 (test X4), while the maximum chord side wall slenderness h_0/t_0 was also 50 (tests X1, X2 and X11). The most slender brace member had a b_1/t_1 value of 50 (tests X4 and X6). Table 4 also indicates whether the connection was loaded in tension (T) or in compression (C).

The test program was designed with the aim of including the complete range of possible failure modes, as identified in the CIDECT references (e.g. Packer et al. 2009), in the experiments: chord face plastification, chord side wall failure, punching shear and effective width failures. Table 5 lists the measured dimensions of all 15 test specimens, with reference to Figs. 4 and 5 for an explanation of the symbols used. In particular, the symbol Δ indicates the maximum imperfection of the chord side wall, measured along the vertical centre line of the connection and averaged over both side walls. A positive value thereby indicates that the side wall bulged outwards. The symbol μ indicates the misalignment between the brace members, as clarified in Figure 5.

Due to the variety of geometries tested, which included both connections loaded in tension and compression, a number of different testing configurations had to be devised. A strong frame with a 1000 kN jack was used to test the smaller size X joints in compression (X1, X2, X3, X5, X7 and X8). The set-up is illustrated in Figure 6a. The specimens were tested between universal hinges, which were fitted onto 320x320x32 mm end plates welded to the braces. This test configuration not only ensured a centred entry of the load into the specimens, but the hinges also allowed for end rotations to develop, mimicking the flexibility of the omitted parts of the brace members and their connections in the actual truss. In particular, the set-up accommodated the increasing in-plane misalignment of the brace members as a result of the chord shear deformations typically observed in X-joints with $\theta \neq 90^o$. This is illustrated for specimen X8 in Figure 6a. At the same time the specimens were short enough to avoid overall Euler buckling.

Specimens X9, X10 and X11 were fabricated of very large size SHS and RHS and were tested in a 2000 kN capacity DARTEC universal testing machine (Fig. 6b). All three specimens were right angle X joints ($\theta = 90^{\circ}$) and were tested between fixed end conditions, a practice which has been common place with various other researchers (e.g. Feng & Young 2010, Rasmussen & Young 2001). After being fitted with welded-on cap plates, the specimens were placed directly on the bed of the testing machine. To bridge the slightly uneven gap between the top cap plate and the plate at the underside of the hydraulic ram, 70 MPa plaster was mixed and sealed inside a plastic bag. The ram was then brought down until it made even contact with the bag and the plaster was left to set before the test.

The X joints in tension (X4 and X6) were tested as illustrated in Figure 6c. Cap plates were welded to the ends of the brace members. Perpendicular plates which could be held by the jaws of the 2000 kN DARTEC universal testing machine were then welded onto the cap plates. The welds in the end plates were designed to be the non-critical components in the test specimens.

Specimens T2 and T3 were tested in tension using the set-up illustrated in Figure 6d. The specimen brace members were fitted with a slotted plate which was placed in the jaws of the 2000 kN capacity DARTEC universal testing machine. Eight 24 mm diameter high-strength threaded rods, doweled into the bed of the machine and connected to RHS100x50x6 cross members, were used to hold the specimen down while a tensile force was applied. The nuts on the eight rods were just loosely tightened without applying any torque. This was done to avoid clamping the specimen down onto the bed, as this would possibly lead to prying action during the test. Instead, the specimen was seen to lift off the bed during the test with a gap of about 2 mm opening up between the underside of the specimen and the base of the machine. This ensured a simple flow of forces where the applied tensile force was transferred by the chord side walls to the reaction points. It is obvious, however, that this set-up can only be used when local failure of the chord member at the reaction points (in particular side wall buckling under the compressive force exerted by the cross members) is not critical.

Specimens T1 and T4 were tested in compression. With β = 0.50, the expected (and observed) failure mode was plastification of the top chord face with very little participation of the side walls. The set-up illustrated in Figure 6e was used. The specimens were placed flat on the bed of the testing machine to prevent any bending moments from developing in the chord and introducing extra compression into the chord top face. The compressive load was introduced into the specimen through a universal hinge to ensure uniform bearing contact with the brace member. T and X joints mainly differ in the way the applied force is transferred by the chord side walls. While in an X joint the force finds its way directly through the side wall to the other side of the connection, a T joint transfers the load in side wall shear. In the proposed set-up the majority of the load is transferred through the side wall into the bed, while also simultaneously spreading out inside the side wall, creating somewhat ambiguous boundary conditions which could be seen as intermediate between those of an X-joint and those of a T-joint. However, since a. failure is localized inside the chord top face, and b. X and T joints are subject to the same design rule for chord face plastification, the proposed set-up was deemed acceptable.

6. **Test results and discussion**

Table 4 summarizes the main experimental findings. Three types of loads were determined from the experiments:

- The maximum load P_u sustained by the connection.

- The 3% deformation limit $P_{3\%}$. This is based on the research by Lu et al. (1994), who proposed (somewhat arbitrarily) to limit the deformations of the connection to 3% of the chord width b_0. This criterion has become an integral part of the CIDECT design philosophy and is implicitly considered in the design equations. In the previously described experiments, this limit was applied to the indentation of the chord face next to the brace member, as well as to the lateral deformation of the chord side wall at the centre of the connection.

- In those cases where side buckling was observed: the buckling load P_{cr}. It should in this context be noted that plates typically possess a significant amount of post-buckling capacity and that local buckling does not lead to immediate collapse. However, local buckling does cause a sudden and severe reduction of the in-plane stiffness of the plate (Marguerre 1937, Hemp 1945). For instance, for a plate simply supported on all four sides the post-buckling stiffness can be shown to be approximately 40% of the initial pre-buckling stiffness. The side wall buckling load of the relevant specimens (X1, X2, X3, X7, X9, X10 and X11) was thus determined by pinpointing this sudden reduction in stiffness in the load vs. axial shortening diagrams. An example is provided in Figure 7. Due to the relatively high h_0/t_0 slenderness values of these specimens, side wall buckling consistently occurred in the elastic range.

While a credible argument can be made to limit the connection capacity to the side wall buckling load P_{cr} in order to avoid non-linear interactive effects between truss member buckling and local buckling of the connection (Becque and Wilkinson 2015), this point of view is not generally accepted and, in line with current CIDECT practice, the capacity of the connection was here determined as the minimum of P_u and $P_{3\%}$ (highlighted in red in Table 4).

Photographs of all failed specimens, together with the relevant load-displacement recordings, are provided in Figs. 7-21.

It was observed that, for the T joints tested in compression (T1 and T4), chord face plastification was the governing failure mode. The 3% b_0 deformation limit turned out to be critical for both joints. The tests were continued until excessive deformations were obtained (equal to a multiple of the 3% b_0 limit) and the load was thereby seen to continually increase (Figs. 7 and 10), but a peak load was not reached.

Joint T2, with a relative small β ratio of 0.38, was tested in tension. Chord face plastification occurred, followed by the 3% b_0 limit being exceeded. However, at a load of 191 kN, a secondary failure occurred by punching shear (Fig. 8).

The remaining T joint T3 was also tested in tension, but this joint had a much larger β ratio of 0.80. This meant that the toes of the welds were sitting right next to the rounded corners of the chord member (Fig. 9). Very little deformation was observed in the connection before it failed in punching shear. The 3% b_0 limit was not critical in this case. It should also be noted that the CIDECT rules only recommend to carry out a check for punching shear when $\beta \geq 0.85$ (Packer et al. 2009). Even when taking punching shear into account, however, the CIDECT rules predicted chord face plastification to be the governing failure mode. This was not observed in the test. As a matter of fact, chord face plastification was physically impossible, since a yield line mechanism could not develop due to the close proximity of the weld toes to the chord side walls.

The 3% b_0 deformation limit was also found to be critical for the X joints in compression failing by chord plastification (X5), side wall buckling (X2, X7, X10 and X11) or a combination of both mechanisms (X1, X8 and X9). Joint X3, which failed by side wall buckling, formed an exception since the peak load was reached before the 3% b_0 deformation limit. In joint X7, local buckling of the brace side walls was also observed. The failure mode was thus a combination of an effective width failure in the braces and side wall buckling in the chord. This can be attributed to the particularly slender nature of the brace walls: b_1/t_1=31.3, which satisfied the CIDECT requirement of a Class 2 section by the narrowest of margins.

It should also be noted that the capacity of joint X10 not only greatly exceeded the CIDECT prediction, but also surpassed the capacity of the test machine (with the maximum recorded load being equal to 1770 kN). Elastic buckling of the side wall was observed, however, before that load was reached.

Joint X6 was loaded in tension and displayed an effective width failure in the brace members. Effective width failures are caused by an uneven stress distribution a result of the fact that the load mostly flows through the brace side walls into the chord side walls, rather than being transferred through the (much more flexible) chord faces. A sudden crack formed in the top brace side wall of the specimen, in the heat-affected zone adjacent to the weld, accompanied by a significant drop in load. The load then increased again while the crack opened up, followed by a second crack suddenly forming in the bottom brace on the opposite side of the connection, which was again located in the heat-affected zone of the weld (Fig.16). This explains the shape of the load-elongation diagram of the specimen in Figure 16. The deformations before failure were insignificant and the failure was sudden and brittle in nature.

Joint X4 included identical (RHS 200x100x4) brace and chord members, connected at a 45^{o} angle. The connection was loaded in tension. Under increasing load, fracture was first observed at both obtuse corners of the brace-chord junction, in the chord material bordering the weld. This was a result of stress concentrations in those particular locations, a phenomenon which is well documented (Packer and Wardenier 1998). The cracks then propagated in the chord along the perimeter of the brace members in a failure which can best be classified as a punching shear failure (Fig. 14). Interestingly, the CIDECT rules state that punching shear can only occur when $\beta \leq 1\text{-}1/\gamma$ (equivalent to $b_1 \leq b_0\text{-}2t_0$), but this experiment demonstrates that this might have to be revised. The CIDECT rules instead predicted an effective width failure in the brace to be the governing failure mode.

7. **Evaluation of the CIDECT design rules**

In order to evaluate the current CIDECT design rules, two predicted capacities were calculated:

- The capacity $P_{CIDECT,1}$ predicted by the current CIDECT rules, taking into account the extra provisions for steel grades up to 460 MPa. This implies that the minimum of f_y and $0.8f_u$ was substituted for f_y in the design equations and an additional factor of 0.9 was applied to the capacity.
- The capacity $P_{CIDECT,2}$ predicted by the current CIDECT rules, valid for steel grades up to 355 MPa, without any modification.

In both cases the measured dimensions and the material properties obtained from the coupon tests were used in the calculations. It is important to note that the CIDECT equations always result in *design* resistances, which already implicitly include a safety factor (Packer et al. 2009). To allow a more direct and objective comparison with the experimental results, the CIDECT predictions $P_{CIDECT,1}$ and $P_{CIDECT,2}$ were first converted to nominal values $P_{pred,1}$ and $P_{pred,2}$, respectively, by multiplying them by the implicit safety factor. This safety factor is γ=1.25 for most failure modes (including punching shear, effective width failures and side wall failure of X-joints), but is γ=1.0 for failure modes involving yielding (chord face plastification) and side wall failure of T-joints (Wardenier 1982).

The predictions $P_{pred,1}$ and $P_{pred,2}$ are listed in Table 4. Table 4 also shows Ratio1, which is the ratio of the experimentally determined capacity (accounting for the 3% deformation limit) to the predicted capacity $P_{pred,1}$, and Ratio2, which is the ratio of the experimentally determined capacity (again including the 3% deformation limit) to the prediction $P_{pred,2}$.

It should be stressed that about half of the test specimens possessed geometric parameters which did not obey the CIDECT limits (most often in terms of wall slenderness) and those connections thus fell outside the range of validity of the current CIDECT rules. Nevertheless, the CIDECT predicted capacities $P_{pred,1}$ and $P_{pred,2}$ of these connections are also listed in Table 4 for the sake of comparison.

A full and conclusive evaluation of whether the current CIDECT rules are safe for grade C450 RHS connections cannot be made at this stage. This would necessarily have to involve the generation of a larger database of results, possibly through finite element modelling and parametric studies, and a proper reliability analysis. This is part of the scope for further research. However, at this stage a comparison of the experimental data against the nominal capacities based on the CIDECT rules points to a number of preliminary conclusions.

First, a quick inspection of the values of Ratio2 for those connections which are within the range of validity of the current CIDECT rules reveals that all values are above 1.0, suggesting that there may not be a need for the additional penalties imposed on C450 steel. The lowest values of Ratio2 are obtained for connections failing by chord face plastification (T1, T2, T4 and X5). They range from 1.44 (T1) down to 1.11 (X5). The often cited rationale for including an additional reduction factor on the capacities of connections in higher strength steel is that larger elastic deformations can be expected before failure and that, therefore, the 3% b_0 limit is expected to become more critical (thus partially or even wholly eliminating the benefits of a higher yield stress). However, the counterargument can be put forward that large deformations are mainly caused by plastification, for instance by the development of a yield line mechanism in the chord face, and that, therefore, an increase in capacity is still to be expected in higher grades steel, even when the 3% b_0 limit governs. While Ratio2 is consistently above 1.0 for those connections satisfying the CIDECT geometric limits, the experimental results also call for some caution. Indeed, it is seen from Table 4 that punching shear is not the failure mode predicted by the CIDECT equations in those cases where it was experimentally observed (joints T3 and X4). In order to make a more relevant comparison, these experimental results are compared to the CIDECT equation for punching shear in Table 6. For joint T3, Ratio2 = 0.86, while for joint X4, Ratio2 = 0.92. This is not entirely surprising, since punching shear is a failure mode which is governed by the tensile strength f_u of the tube material, while the CIDECT equation is based on the yield strength f_y. The reader is thereby reminded that the f_u/f_y ratio of the C450 material did not meet the CIDECT recommended minimum value of 1.2 (albeit by a small margin). A similar observation can be made for connection X6, where Ratio2 = 0.85. Connection X6 underwent an effective width failure, displaying fracture in tension, a phenomenon equally governed by f_u (although it should be mentioned for completeness that the b_1/t_1 ratio of the brace lay outside the CIDECT slenderness limit). The T3, X4 and X6 test results seem to suggest that modifications to the CIDECT rules may be justified for C450 connections for those failure modes involving fracture (i.e. punching shear and effective width failures in tension), although it is again stressed that more data is needed, accompanied by a reliability analysis, to draw final conclusions. The authors also propose to base the design equations for punching shear and effective width failure in tension on the tensile strength f_u, rather than the yield stress f_y, and make the safety explicit, in order to eliminate the dependence of the design equations on the f_u/f_y ratio.

The highest values of Ratio2 were obtained for the connections with β = 1.0, which failed by side wall buckling, with values ranging from a minimum of 1.9 to even 3.6. Interestingly, the highest values were obtained for the most slender sidewalls, indicating that the current CIDECT rule for side wall buckling is overly conservative, and more so as the wall slenderness increases. In principle, the results show that the range of validity of the current rule for side wall buckling could easily be extended to a wall slenderness of 50. On this issue it is worth mentioning that Becque and Cheng (2016) have proposed an alternative design equation for this type of failure, which is more accurate than the current CIDECT rule throughout the whole slenderness range and which is valid for steel grades up to 450MPa. The results of test X7 also indicate that, in case the brace members display h_1/t_1 values beyond the Class 2 limit, the brace walls may participate in the buckling pattern, resulting in a dramatically reduced value for Ratio2 (= 1.18).

All connections tested in compression with a side wall slenderness in excess of the CIDECT limit of 40 and $\beta < 1.0$ (joints X1, X8 and X9) were observed to fail by a combination of chord face plastification and side wall buckling. These tests reveal that:

- due to the limited bending stiffness of the walls, interaction between the two failure modes becomes prominent for β values much lower than the current CIDECT limit of 0.85 (for instance, β=0.60 in joint X8).
- this type of combined failure results in much reduced capacities with Ratio1 and Ratio2 values below 1.0 (Ratio1=0.84 for X1 and Ratio1=0.87 for X8). The value of Ratio1=0.87 for X8 is somewhat worrying since the wall slenderness of the chord, at 42, is only slightly outside the current CIDECT limit of 40. It is thought that the in-plane shear deformations in the chord (Fig. 5a) might in this case have contributed to a reduced failure load.

Consequently, the current CIDECT rules should not be applied to these connections and more research is needed to develop appropriate design equations for connections with slender chord walls and $\beta < 1.0$.

8. **Conclusions**

In this paper the results of an experimental investigation into the static capacity of grade C450 SHS/RHS truss connections are presented. The experimental program included four tests on T joints and 11 tests on X joints. A wide range of geometries was considered, including some which did not meet the limits of the current CIDECT rules (particularly in terms of wall slenderness), but nevertheless consisted of commercially available sections. Material properties were measured and are reported in the paper. Of particular interest is the f_u/f_y ratio, which was calculated to be, on average, 1.17. This is slightly below the minimum value of 1.2, imposed by the CIDECT rules.

The experimental results led to preliminary indications that:

- the limiting range of $0.85 \leq \beta \leq 1\text{-}1/\gamma$, in which punching shear needs to be checked according to the CIDECT rules, needs to be revised, since punching shear failures were observed outside this range, both for lower and higher β values.
- there is currently no experimental evidence to justify the introduction of an additional penalty factor of 0.9 for grade C450 T and X connections failing in ductile modes, provided the geometric constraints imposed on the CIDECT provisions are satisfied. In particular, the CIDECT equations valid for grades up to 355 MPa predict safe capacities for C450 joints failing by chord face plastification and side wall buckling.
- there is, however, experimental evidence to introduce reduction factors in the CIDECT equations for connections failing by fracture, in particular for: a. punching shear, and b. effective width failures in tension.
- the current CIDECT equations for side wall buckling are conservative and become more conservative as the side wall slenderness increases.

- more research is necessary for connections with chords falling outside the current CIDECT wall slenderness limit and $\beta < 1.0$. The current CIDECT rules should not be applied to these connections.

Acknowledgment

This research was made possible thanks to the financial support of CIDECT (under project 5BV) and OneSteel Australian Tube Mills. Australian Tube Mills also generously donated the materials used in the experimental program.

REFERENCES

AS/NZS 1163 (2009). "Cold-formed structural steel hollow sections." Australian Standard/New Zealand Standard, Standards Australia, Sydney, Australia.

AS/NZS 1391 (1991). "Methods for Tensile Testing of Metals." Australian Standard/New Zealand Standard 1391:1991, Standards Australia, Sydney, Australia.

AS/NZS 1554.1 (2000). "Structural steel welding: Part 1: Welding of steel structures." Australian Standard/New Zealand Standard, Standards Australia, Sydney, Australia.

Becque, J., and Cheng, S. (2016). "Side wall buckling of equal-width RHS truss X-joints" *Journal of Structural Engineering*, ASCE, under review.

Becque, J., and Wilkinson, T. (2015). "A new design equation for side wall buckling of RHS truss X-joints." 15th International Symposium on Tubular Structures, Rio de Janeiro, Brazil; in *Tubular Structures XV*, eds. Batista, E., Vellasco, P., and Lima, L., CRC Press, pp. 419-426.

Becque, J., Wilkinson, T., and Syam, A. (2011). "Experimental investigation of X and T truss connections in C450 cold-formed rectangular hollow sections." CIDECT report 5BV.

EN 1990 (EC0) (2002). "Eurocode 0: Basis of structural design." European Committee for Standardization, Brussels, Belgium.

EN 1993-1-1 (EC3) (2005). "Eurocode 3: Design of steel structures – Part 1.1: General rules." European Committee for Standardization, Brussels, Belgium.

EN 1993-1-8 (EC3) (2005). "Eurocode 3: Design of steel structures – Part 1.8: Design of joints." European Committee for Standardization, Brussels, Belgium.

Feng, R., and Young, B. (2010). “Tests and behaviour of cold-formed stainless steel tubular X-joints.” *Thin-Walled Structures* 48(12), pp. 921-934.

Fleischer, O., and Puthli, R. (2008). “Extending existing design rules in EN1993-1-8 (2005) for gapped RHS K-joints for maximum chord slenderness b_0/t_0 of 35 to 50 and gap size g to as low as $4t_0$.” 12th International Symposium on Tubular Structures, Shanghai, China; in *Tubular Structures XII*, eds. Shen, Z.Y., Chen, Y.Y., and Zhao, X.Z., CRC Press, pp. 293-301.

Hemp, W.S. (1945). "The theory of flat panels buckled in compression," Aeronautical Research Council, *Reports and Memoranda*.

IIW (2009). “Static design procedure for welded hollow section joints – Recommendations.” 3rd edition, International Institute of Welding, Sub-commission XV-E, Annual Assembly, Singapore, *IIW Doc. XV-1329-09*.

Koning, C.H.M., de, and Wardenier, J. (1976). “Supplement with test results of welded joints in structural hollow sections with rectangular boom.” *TNO-IBBC Report No. BI-76-122/35.3.51210. Stevin Report No. 6-76-5.*

Kurobane, Y. (1981). “New developments and practices in tubular joint design.” *IIW Doc. XV-488-81* and *IIW Doc. XIII-1004-81*.

Liu, D.K., and Wardenier, J. (2004). “Effect of the yield strength on the static strength of uniplanar K-joints in RHS (steel grades S460, S355 and S235).” *IIW Doc. XV-E-04-293*, Delft University of Technology, Delft, The Netherlands.

Lu, L.H., de Winkel, G.D., Yu, Y., and Wardenier, J. (1994). “Deformation limit for the ultimate strength of hollow section joints.” *Proceedings of the 6th International Symposium on Tubular*

Structures, Melbourne, Australia, Tubular Structures VI, Balkema, Rotterdam, The Netherlands, pp. 341-347.

Mang, F. (1978). “Untersuchungen an Verbindungen von geschlossenen und offenen Profilen aus hochfesten Stählen.” AIF-Nr. 3347. Universität Karlsruhe, Germany.

Marguerre, K. (1937). "The apparent width of the plate in compression." *Luftfahrtforschung,* 14 (3).

Noordhoek, C., Verheul, A., Foeken, R.J., Bolt, H.M., and Wicks, P.J. (1996). “Static strength of high strength steel tubular joints.” *ECSC agreement number 7210-MC/602*.

Packer, J.A., Sherman, D., and Lecce, M. (2010). Hollow Structural Section Connections, AISC Steel Design Guide 24, American Institute of Steel Construction, USA.

Packer, J.A., and Wardenier, J. (1998). “Stress concentration factors for non-90^{o} X-connections made of square hollow sections.” Canadian Journal of Civil Engineering, 25, pp. 370-375.

Packer, J.A., Wardenier, J., Zhao, X.-L., van der Vegte, G.J., Kurobane, Y. (2009). *Design guide for rectangular hollow section (RHS) joints under predominantly static loading.* Second edition, CIDECT series “Construction with hollow steel sections” No. 3, Verlag TUV Rheinland, Köln, Germany.

Puthli, R., Bucak, O., Herion, S., Fleischer, O., Fischl, A., and Josat, O. (2010). “Adaptation and extension of the valid design formulae for joints made of high-strength steels up to S690 for cold-formed and hot-rolled sections.” *CIDECT report 5BT-7/10* (draft final report), Germany.

Rasmussen, K.J.R., and Young, B. (2001). “Tests of X- and K-joints in SHS stainless steel tubes.” *Journal of Structural Engineering* 127 (10), pp.1173-1182.

Wardenier, J. (1982). *Hollow Section Joints*, Delft University Press, the Netherlands.

Wardenier, J., Packer, J.A., Choo, Y.S., van der Vegte, G.J, and Orton, A. (2009). "Axially loaded T and X joints of elliptical hollow sections" *CIDECT report 5BW-6/09*.

Wardenier, J., and Puthli, R. (2011). "Korreturvorschläge für die DIN EN 1993-1-8 zum Thema Hohlprofilanschlüsse." *Stahlbau*, 80, pp. 470-482.

Yu, Y. (1997). "The static strength of uniplanar and multiplanar connections in rectangular hollow sections." PhD thesis, Delft University Press, Delft, The Netherlands.

Table 1. Commercial SHS outside the CIDECT slenderness limit

Section	b (mm)	t (mm)	b/t
SHS 350x350x8	350	8	43.8
SHS 250x250x6	250	6	41.7
SHS 100x100x2	100	2	50.0
SHS 89x89x2	89	2	44.5
SHS 65x65x1.6	65	1.6	40.6

Table 2. Commercial RHS outside the CIDECT slenderness limit

Section	max(b, h) (mm)	t (mm)	max(b, h)/t
RHS 400x300x8	400	8	50.0
RHS 400x200x8	400	8	50.0
RHS 350x250x8	350	8	43.8
RHS 350x250x6	350	6	58.3
RHS 300x200x6	300	6	50.0
RHS 250x150x6	250	6	41.7
RHS 250x150x5	250	5	50.0
RHS 200x100x4	200	4	50.0
RHS 150x50x3	150	3	50.0
RHS 150x50x2.5	150	2.5	60.0
RHS 150x50x2	150	2	75.0
RHS 125x75x3	125	3	41.7
RHS 125x75x2.5	125	2.5	50.0
RHS 125x75x2	125	2	62.5
RHS 100x50x2	100	2	50.0
RHS 100x50x1.6	100	1.6	62.5
RHS 75x50x1.6	75	1.6	46.9
RHS 75x25x1.6	75	1.6	46.9

Table 3. Tensile coupon test results

		Adjacent to weld		Opposite weld	
Section	Source	f_y (MPa)	f_u (MPa)	f_y (MPa)	f_u (MPa)
400x400x16	JAP*	478	527	434	531
400x300x8	JAP	446	542	469	550
350x350x8	JAP	441	524	443	514
350x250x10	JAP	432	534	455	534
300x300x8	JAP	471	536	462	510
250x250x6	JAP	476	562	504	574
250x150x5	AUS*	426	509	449	518
200x200x6	AUS	442	516	456	524
200x100x5	AUS	425	495	440	534
200x100x4	AUS	422	508	453	523
150x150x6	AUS	432	499	433	504
125x125x5	AUS	424	503	418	502
Average JAP		457	538	461	536
Average AUS		428	505	441	518

* JAP = Japanese origin; AUS = Australian origin.

Table 4. Test program and results

Test	Chord	Brace	β	2γ	τ	α	T/C [1]	Predicted failure mode	Observed failure mode	P_{cr} [2]	P_u [3]	$P_{3\%}$ [4]	$P_{pred,1}$ [5]	$P_{pred,2}$ [6]	Ratio 1 [7]	Ratio 2 [8]
-	-	-	-	-	-	°	-	-	-	kN	kN	kN	kN	kN	-	-
T1	200x200x6	100x100x8	0.50	33	1.33	90	C	Chord face plastification	Chord face plastification	-	Not reached	171	99	119	1.73	1.44
T2	200x200x6	75x75x5	0.38	33	0.83	90	T	Chord face plastification	Chord face plastification	-	191	118	79	95	1.49	1.24
T3	125x125x5	100x50x6	0.80	25	1.20	90	T	Chord face plastification	Punching shear	-	217	Not reached	105	122	2.07	1.78
T4	400x400x16	200x200x12.5	0.50	25	0.78	90	C	Chord face plastification	Chord face plastification	-	Not reached	1075	740	885	1.45	1.21
X1	250x150x5	125x125x5	0.83	30	1.00	90	C	Chord face plastification	Chord side wall buckling +chord face plastification	164	251	181	182	215	0.99	0.84
X2	250x150x5	150x150x5	1.00	30	1.00	90	C	Chord side wall buckling	Chord side wall buckling	250	413	365	106	118	3.44	3.09
X3	150x150x6	150x150x6	1.00	25	1.00	90	C	Chord side wall buckling	Chord side wall buckling	628	831	Not reached	384	439	2.16	1.89
X4	200x100x4	200x100x4	1.00	50	1.00	45	T	Effective width failure	Punching shear	-	588	Not reached	482	567	1.22	1.04
X5	200x100x5	150x100x5	0.75	40	1.00	45	C	Chord face plastification	Chord face plastification	-	226	223	172	201	1.30	1.11
X6	200x200x6	200x100x4	1.00	33	0.67	90	T	Effective width failure	Effective width failure	-	659	Not reached	655	779	1.01	0.85
X7	150x150x6	125x125x4	0.83	25	0.67	90	C	Chord face plastification	Side wall failure +effective width failure	200	356	350	248	296	1.41	1.18
X8	250x250x6	150x150x6	0.60	42	1.00	60	C	Chord face plastification	Chord side wall buckling + chord face plastification	-	202	181	174	208	1.04	0.87
X9	350x350x8	300x300x8	0.86	44	1.00	90	C	Chord side wall buckling + chord face plastification	Chord side wall buckling + chord face plastification	465	848	735	498	588	1.48	1.25
X10	350x250x10	250x250x10	1.00	25	1.00	90	C	Chord side wall buckling	Chord side wall buckling	1336	>1770	>1770	676	756	>2.62	>2.34
X11	400x300x8	300x300x8	1.00	38	1.00	90	C	Chord side wall buckling	Chord side wall buckling	670	1291	1270	320	356	3.97	3.57

[1] T/C = Tension/Compression
[2] P_{cr} = Experimentally measured buckling load of the chord side wall
[3] P_u = Experimentally measured ultimate load

[4] $P_{3\%}$ = Experimentally measured load where the chord deformations exceed 3% of the chord width
[5] $P_{pred,1}$ = Predicted capacity using the minimum value of f_y and $0.8f_u$ and an additional reduction factor of 0.9
[6] $P_{pred,2}$ = Predicted capacity using only f_y without an additional reduction factor of 0.9
[7] Ratio1 = $\min(P_u, P_{3\%}) / P_{pred,1}$
[8] Ratio2 = $\min(P_u, P_{3\%}) / P_{pred,2}$

Table 5. Specimen dimensions

Specimen	h_0	b_0	t_0	r_0	h_1	b_1	t_1	r_1	θ_1	θ_2	Δ	μ	H	L
	(mm)	(mm)	(mm)	(mm)	(mm)	(mm)	(mm)	(mm)	-	-	(mm)	(mm)	(mm)	(mm)
T1	200.00	198.90	5.85	19.1	99.90	100.35	8.04	17.7	90.1	-	1.0	-	898	1210
T2	199.00	199.50	5.81	17.0	75.18	75.09	4.94	10.9	90.2	-	0.5	-	1001	1208
T3	124.84	124.85	4.73	8.7	49.94	100.03	5.94	11.3	90.0	-	-0.5	-	927	1214
T4	400.30	400.50	15.95	39.5	199.80	199.50	12.35	30.7	89.7	-	1.5	-	1400	1198
X1	248.50	149.85	4.95	15.9	125.25	125.25	4.83	10.8	89.7	89.6	2.0	2.0	1550	1505
X2	250.00	149.77	5.00	17.7	150.10	150.10	4.76	11.4	90.2	89.7	3.0	2.0	1752	1503
X3	150.18	150.23	5.86	14.1	150.48	150.35	5.86	14.7	90.2	90.0	-1.0	0.0	1653	1505
X4	100.60	198.70	3.93	8.7	100.60	198.70	3.93	8.7	44.8	135.6	-0.5	2.0	1550	1508
X5	100.11	199.20	4.87	11.1	100.25	150.08	4.95	10.9	44.3	136.2	-1.0	4.0	1552	1380
X6	199.50	199.50	5.83	17.5	100.60	198.70	3.93	8.7	90.3	90.5	1.0	2.0	1602	1406
X7	150.10	150.12	5.88	13.9	125.58	125.05	3.93	9.3	89.7	90.4	-0.5	1.0	1462	1505
X8	249.40	249.00	6.10	19.1	150.54	150.42	5.85	13.3	59.7	120.0	1.8	10.0	1705	1498
X9	350.90	349.80	7.88	24.3	300.30	300.30	7.97	22.3	90.2	92.4	1.5	0.0	2241	2501
X10	350.40	250.70	9.94	27.0	248.50	249.00	9.94	26.6	90.0	89.9	0.0	0.0	2238	2499
X11	400.00	300.00	7.92	22.7	300.30	300.30	7.97	22.3	90.1	90.1	2.0	0.0	2242	2497

Table 6. Punching shear: comparison with CIDECT design equation

Test	P_u	$P_{pred,1}$	$P_{pred,2}$	Ratio1	Ratio2
	kN	kN	kN	-	-
T3	217	217	252	1.00	0.86
X4	588	637	540	1.09	0.92

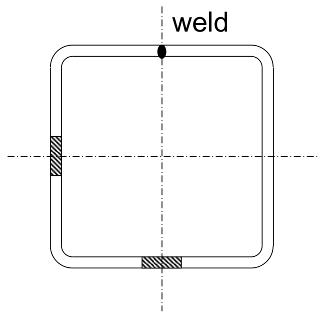

Figure 1. Location of the test coupons.

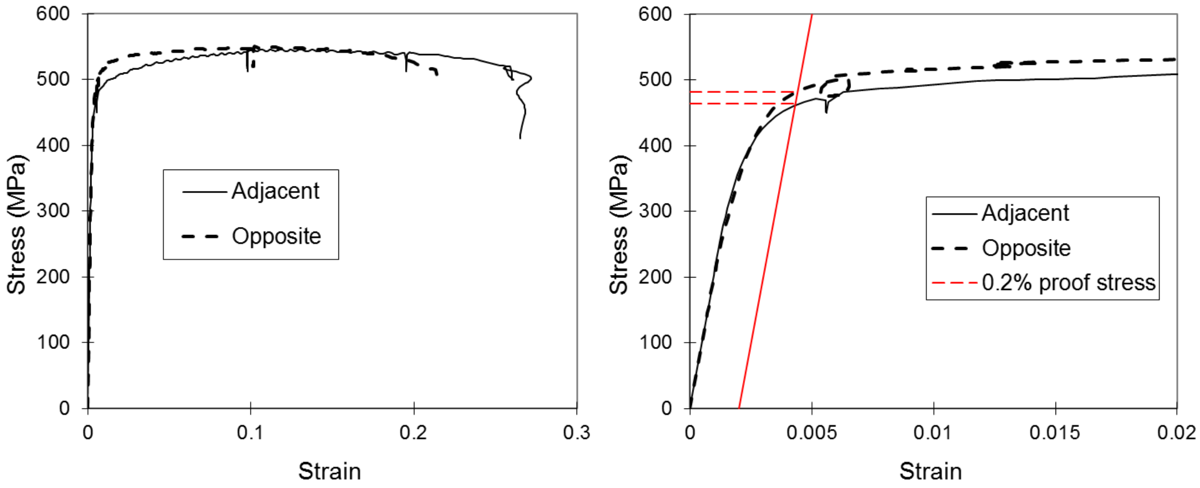

Figure 2. SHS200x200x6 coupon test results: a. full stress-strain curve, b. initial portion up to 2% strain.

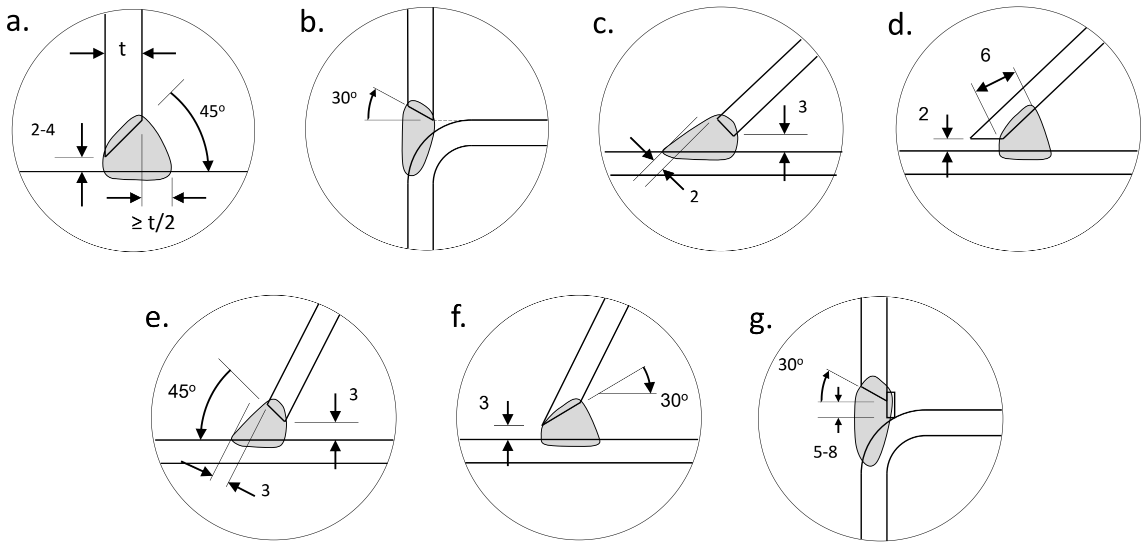

Figure 3. Weld details (dimensions in mm)

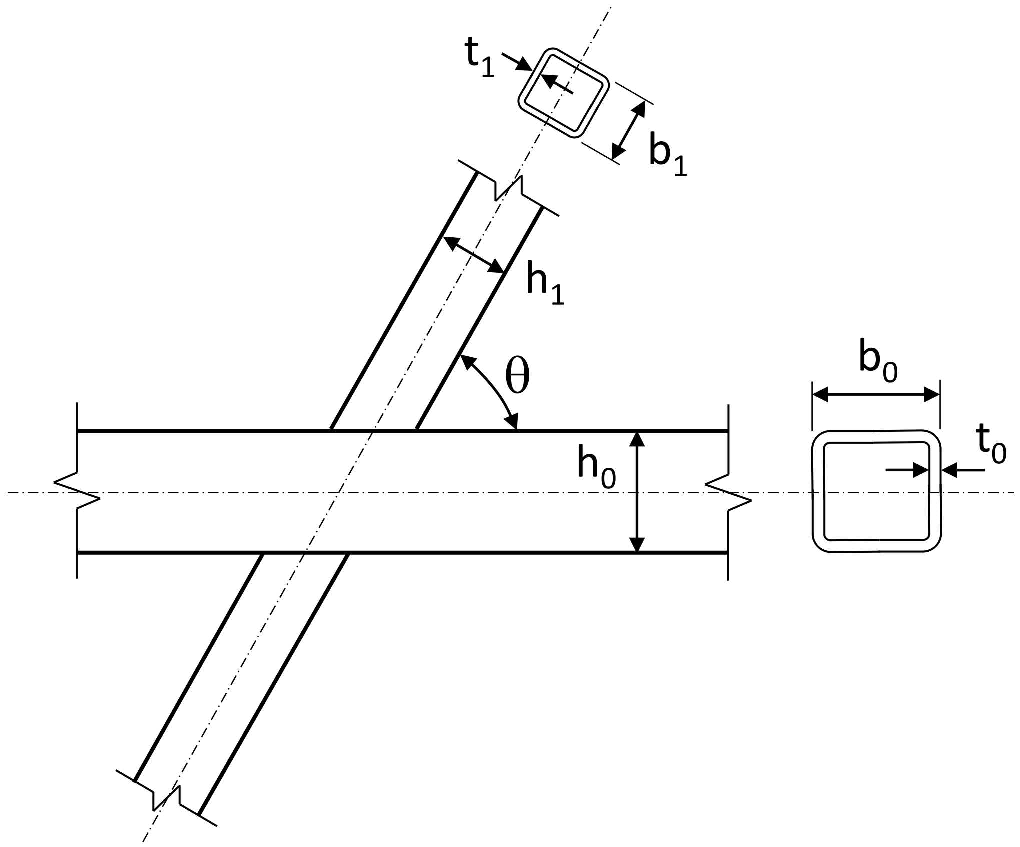

Figure 4. Connection geometry

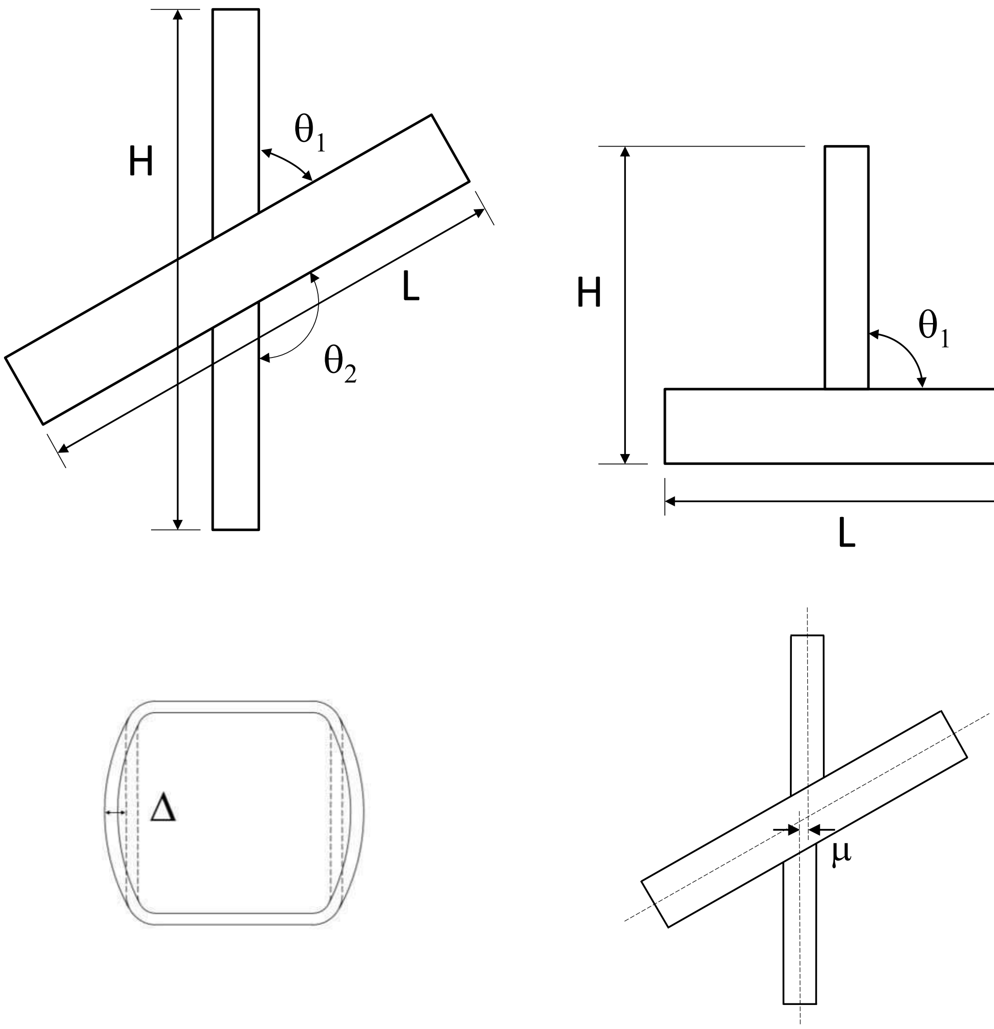

Figure 5. Overall dimensions and imperfections

Figure 6. Test configurations

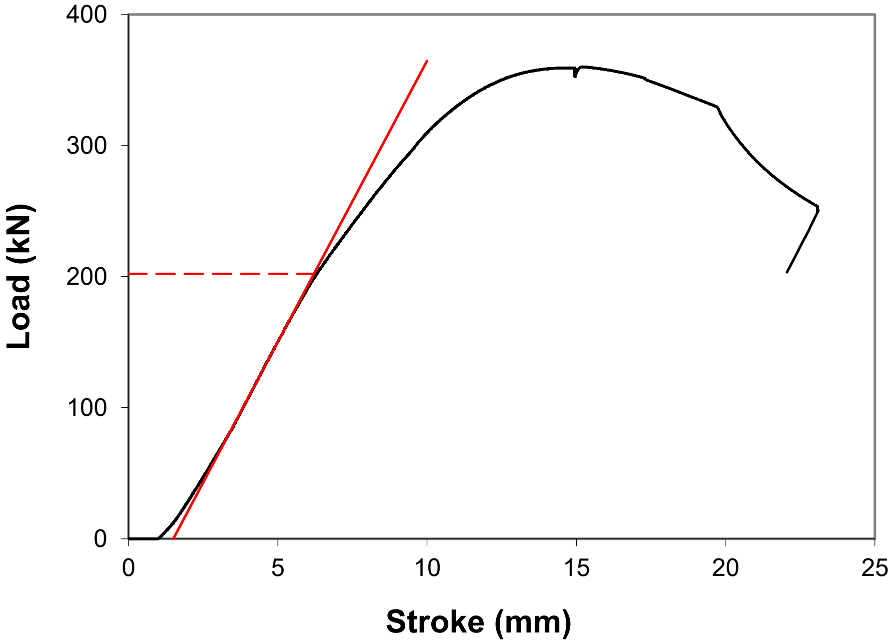

Figure 7. Determination of the side wall buckling load

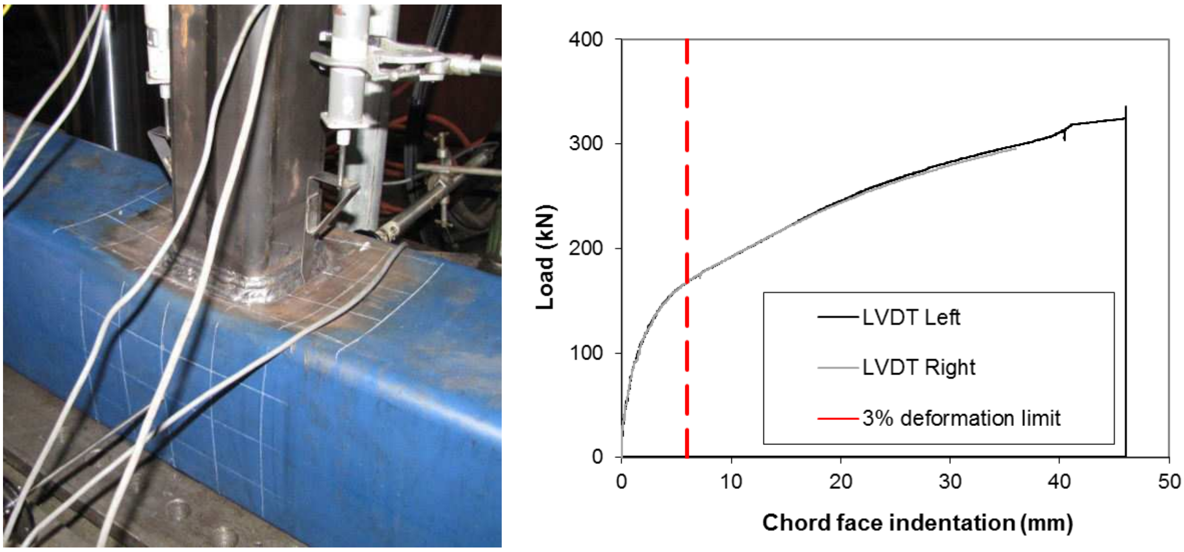

Figure 8. Test T1: failure mode and load-deformation behaviour

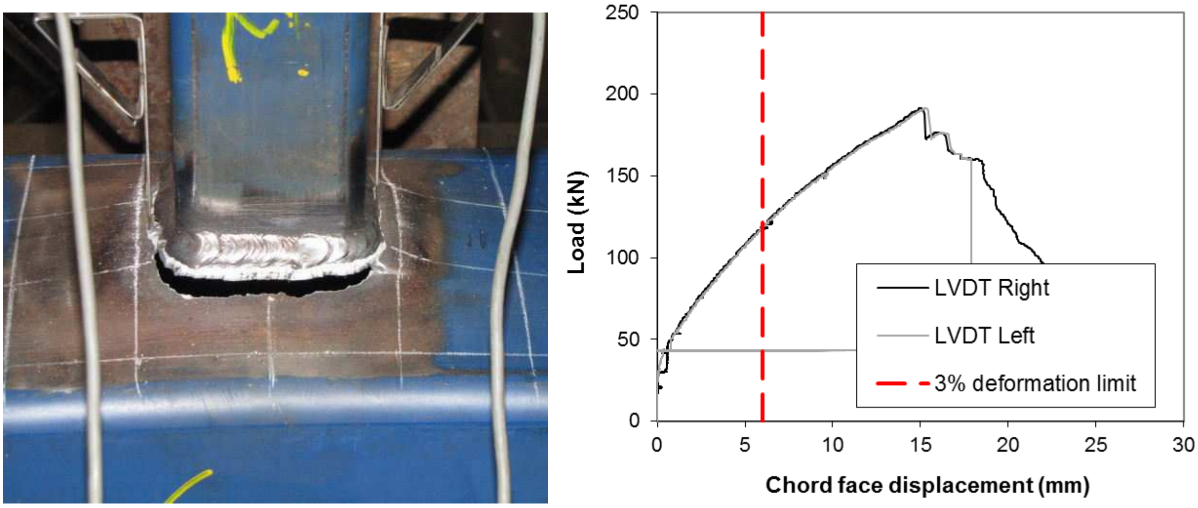

Figure 9. Test T2: failure mode and load-deformation behaviour

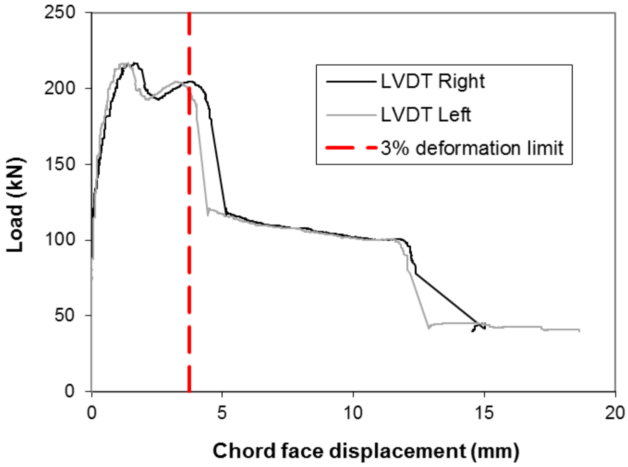

Figure 10. Test T3: failure mode and load-deformation behaviour

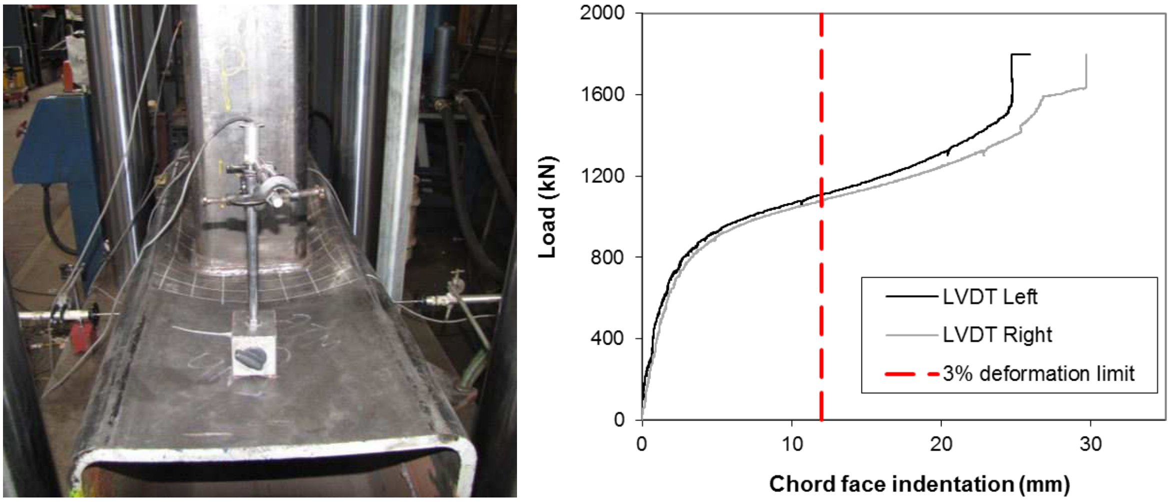

Figure 11. Test T4: failure mode and load-deformation behaviour

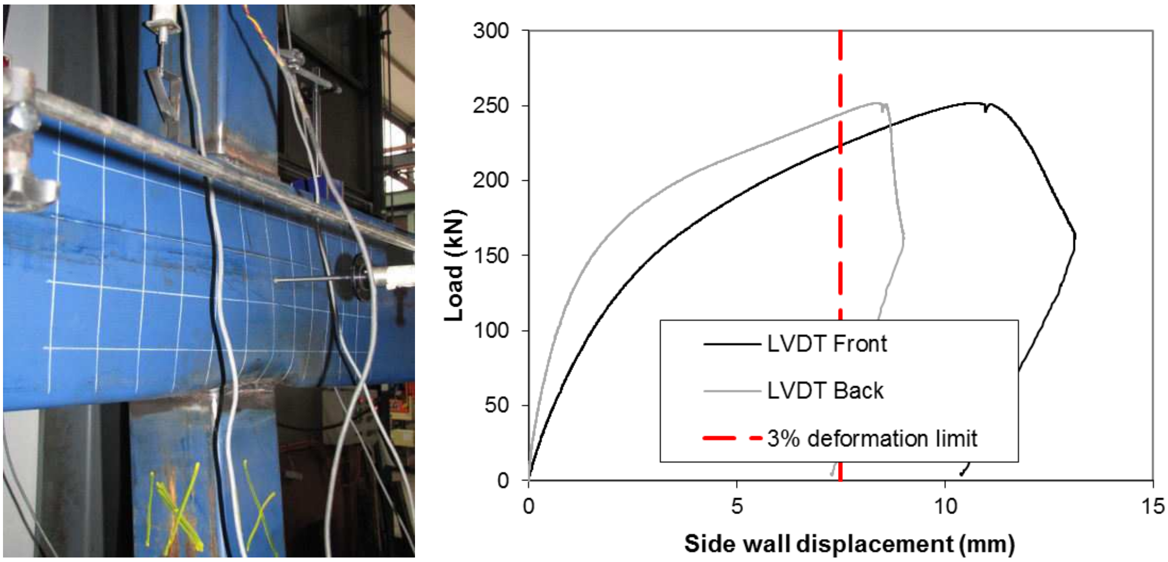

Figure 12. Test X1: failure mode and load-deformation behaviour

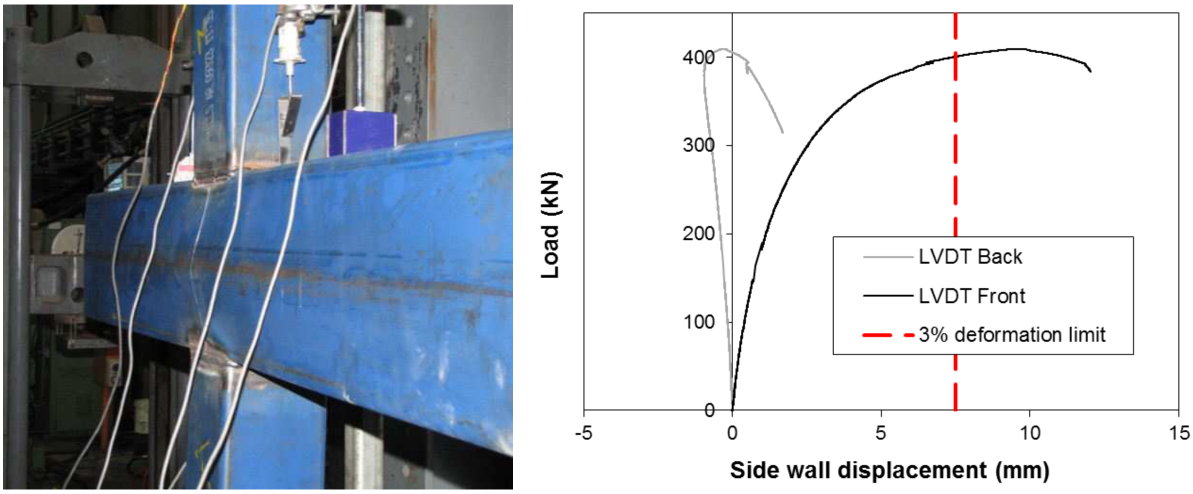

Figure 13. Test X2: failure mode and load-deformation behaviour

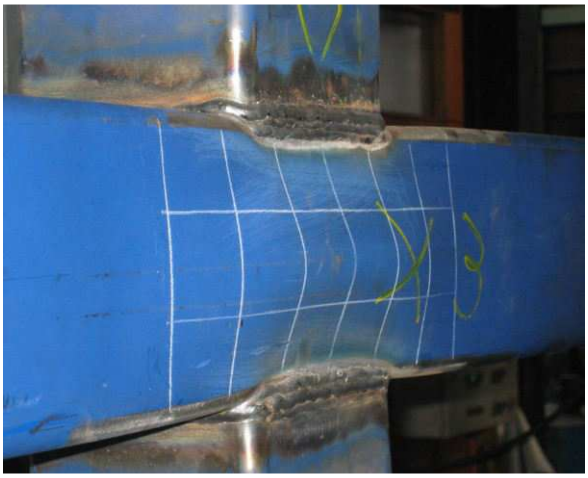

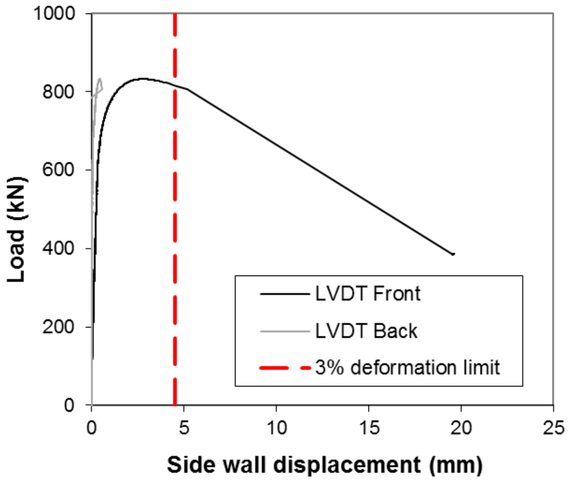

Figure 14. Test X3: failure mode and load-deformation behaviour

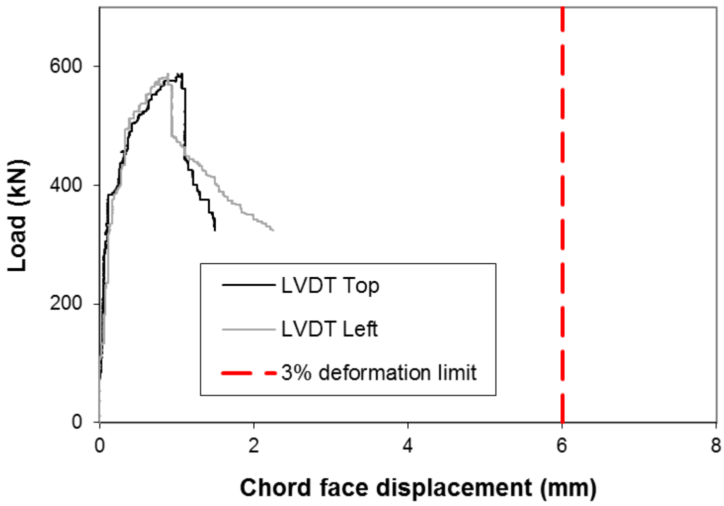

Figure 15. Test X4: failure mode and load-deformation behaviour

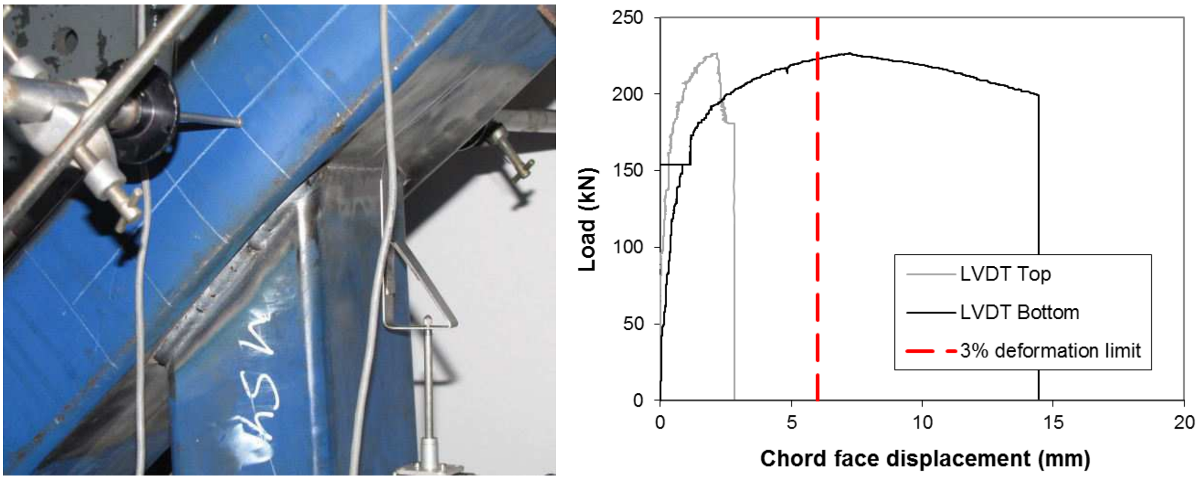

Figure 16. Test X5: failure mode and load-deformation behaviour

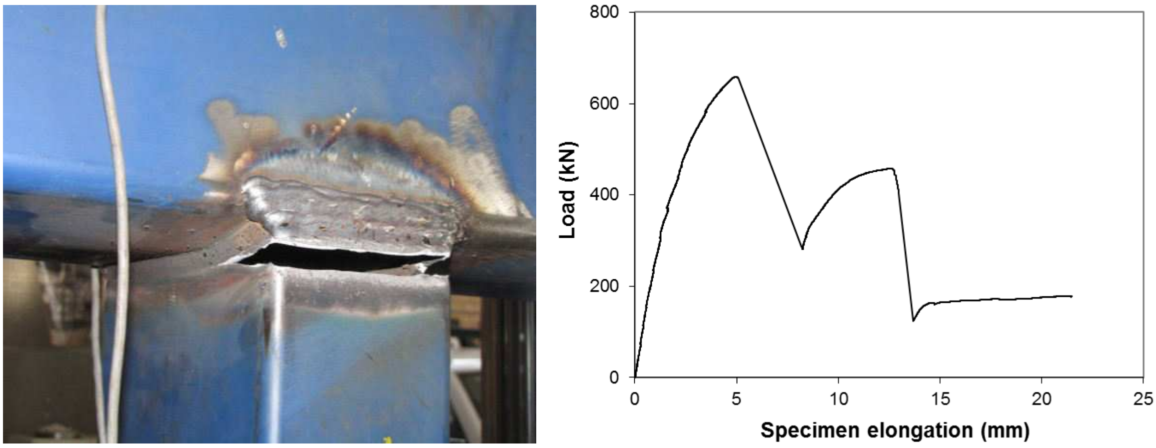

Figure 17. Test X6: failure mode and load-deformation behaviour

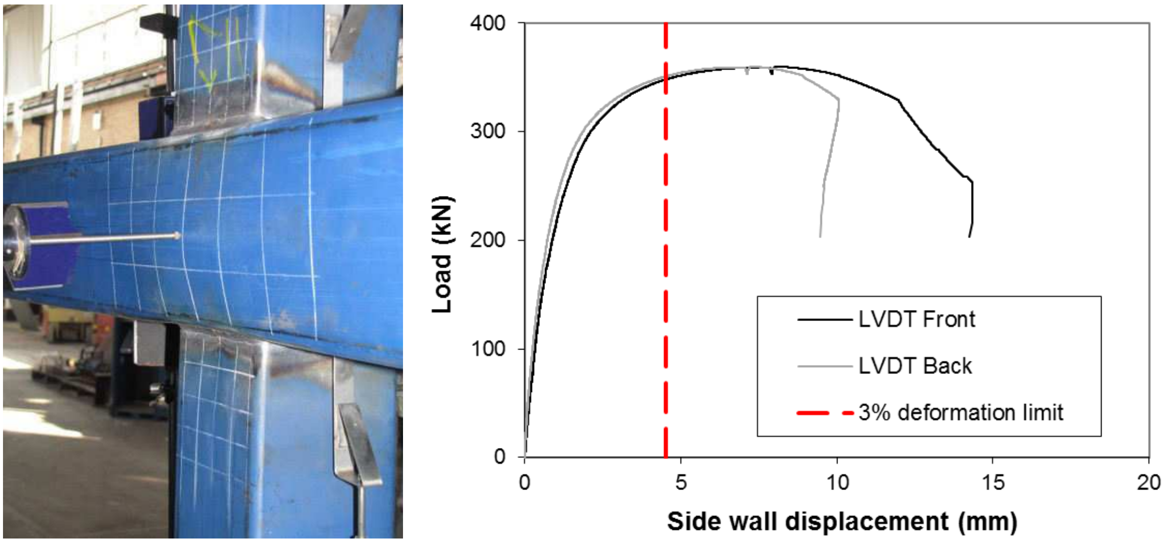

Figure 18. Test X7: failure mode and load-deformation behaviour

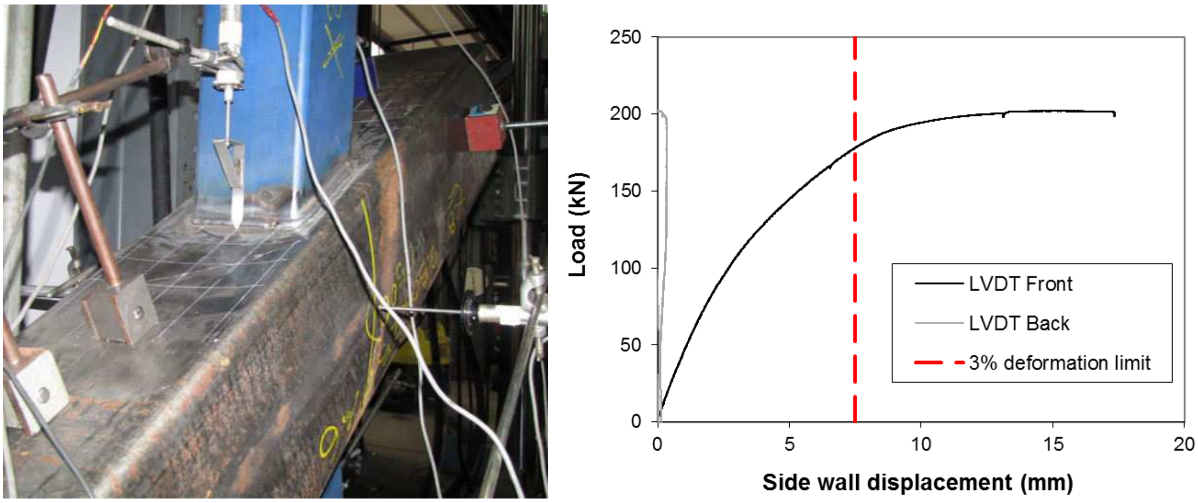

Figure 19. Test X8: failure mode and load-deformation behaviour

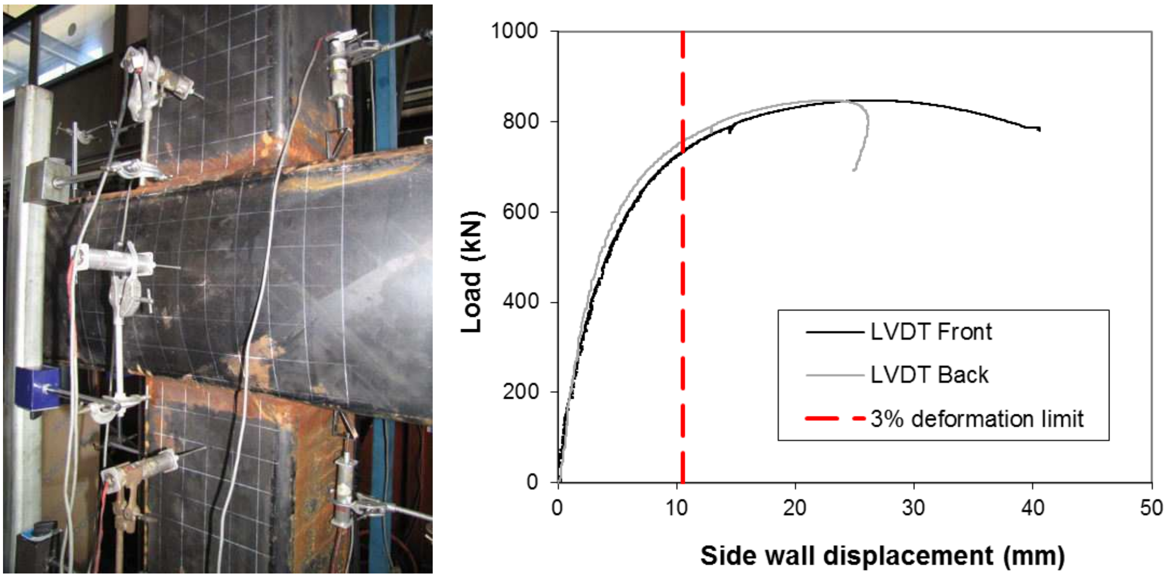

Figure 20. Test X9: failure mode and load-deformation behaviour

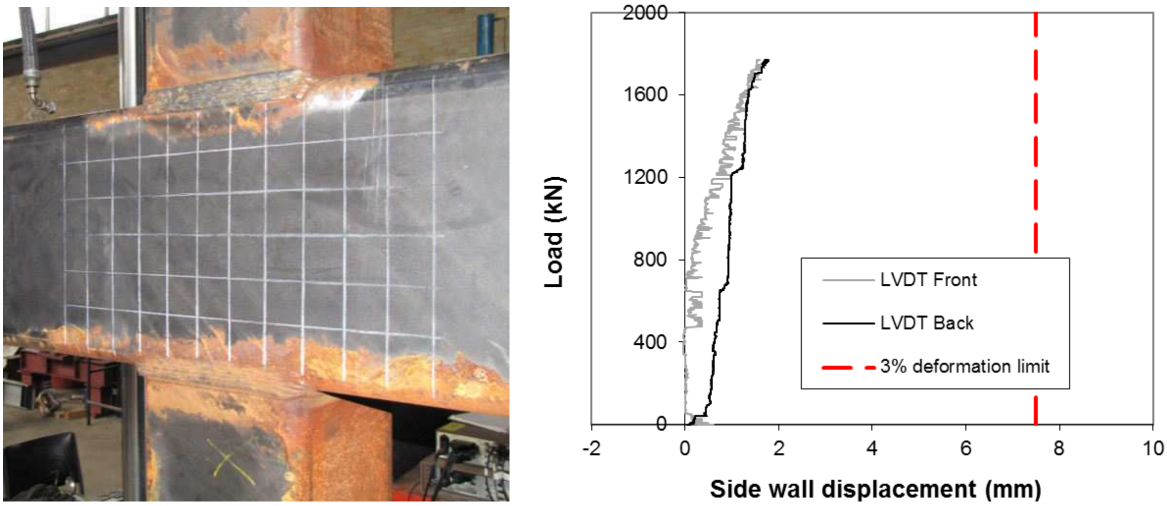

Figure 21. Test X10: failure mode and load-deformation behaviour

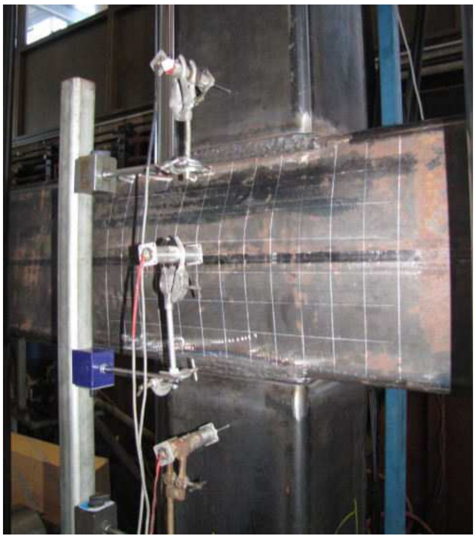

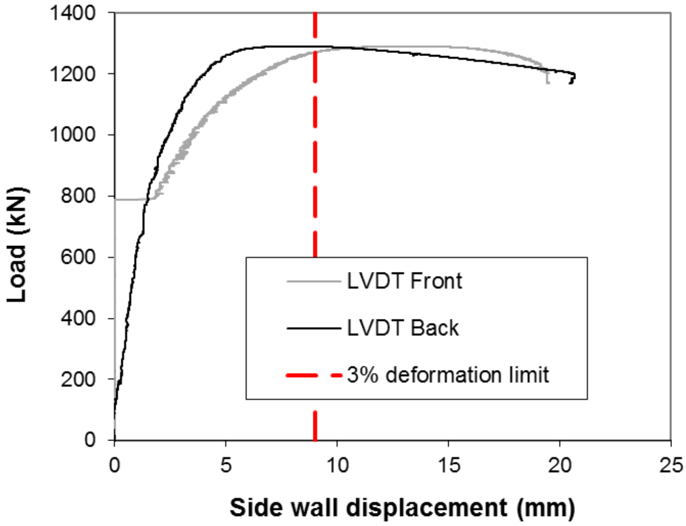

Figure 22. Test X11: failure mode and load-deformation behaviour